Full-Field and Scanning Microtomography Based on Parabolic Refractive X-Ray Lenses

C. G. Schroer[a], M. Kuhlmann[b], T. F. Günzler[c], B. Benner[c], O. Kurapova[c], J. Patommel[a], B. Lengeler[c], S. V. Roth[b], R. Gehrke[b], A. Snigirev[d], I. Snigireva[d], N. Stribeck[e], A. Almendarez-Camarillo[e], F. Beckmann[f]

[a]Institute of Structural Physics, Dresden University of Technology, D-01062 Dresden, Germany
[b]HASYLAB at DESY, Notkestr. 85, D-22607 Hamburg, Germany
[c]II. Physikalisches Institut, Aachen University, D-52056 Aachen, Germany
[d]ESRF, PB 220, F-38043 Grenoble, Cedex, France
[e]Inst. Tech. & Mol. Chem., Hamburg University, Bundesstr. 45, D-20146 Hamburg, Germany
[f]GKSS-Research Center at DESY, Notkestr. 85, D-22607 Hamburg, Germany

ABSTRACT

Hard x-ray full field and scanning microscopy both greatly benefit from recent advances in x-ray optics. In full field microscopy, for instance, rotationally parabolic refractive x-ray lenses can be used as objective lens in a hard x-ray microscope, magnifying an object onto a detector free of distortion. Using beryllium as lens material, a hard x-ray optical resolution of about 100 nm has been obtained in a field of view of more than 500 micrometers. Further improvement of the spatial resolution to below 50 nm is expected. By reconstructing the sample from a series of micrographs recorded from different perspectives, tomographic imaging with a resolution well below one micrometer was achieved. The technique is demonstrated using a microchip as test sample. In scanning microscopy and tomography, the sample is scanned through a hard x-ray microbeam. Different hard x-ray analytical techniques can be exploited as contrast mechanism, such as x-ray fluorescence, absorption, or scattering. In tomographic scanning mode, they yield for example local elemental, chemical, or structural information from inside a specimen. At synchrotron radiation sources, a small and intensive microbeam can be generated by imaging the source onto the sample position in a strongly reducing geometry, e. g., by parabolic refractive x-ray lenses. With nanofocusing refractive x-ray lenses, a lateral beamsize of 50 nm was reached. As an example for scanning tomography, we consider tomographic small angle x-ray scattering (SAXS-tomography), reconstructing a series of SAXS patterns related to small volume elements inside a polymer rod made by injection moulding.

Keywords: hard x-ray microscopy, x-ray nanoprobe, tomography, small-angle x-ray scattering, refractive x-ray optics

1. INTRODUCTION

One of the key strength of hard x-ray microscopy is the large penetration depth of hard x-rays in matter. As opposed to visible light, electrons, or scanning probes, hard x-rays can probe deeply into the interior of a specimen. Tomographic scanning techniques allow one to reconstruct the 3-dimensional inner structure. Microscopic imaging with hard x-rays is possible using different schemes, such as full-field and scanning microscopy.

Full-field microscopy with hard x-rays in projection (radiography) is limited in spatial resolution by source size and detector resolution. Figure 1(a) shows this scheme. Since the spatial resolution of hard x-ray detectors is currently limited to slightly below 1μm, magnifying schemes using a small secondary source are needed to increase the spatial resolution to well below this limit. Such a small focus can for example be generated by imaging a synchrotron radiation source onto the focus position by an x-ray optic, such as a Kirkpatrick-Baez mirror system, a Fresnel zone plate, or a refractive x-ray lens. Alternatively, an x-ray optic, such as a Fresnel

Further author information: (Send correspondence to C. G. Schroer.)
C. G. Schroer: E-mail: schroer@xray-lens.de, Telephone: +49 (351) 463 37589

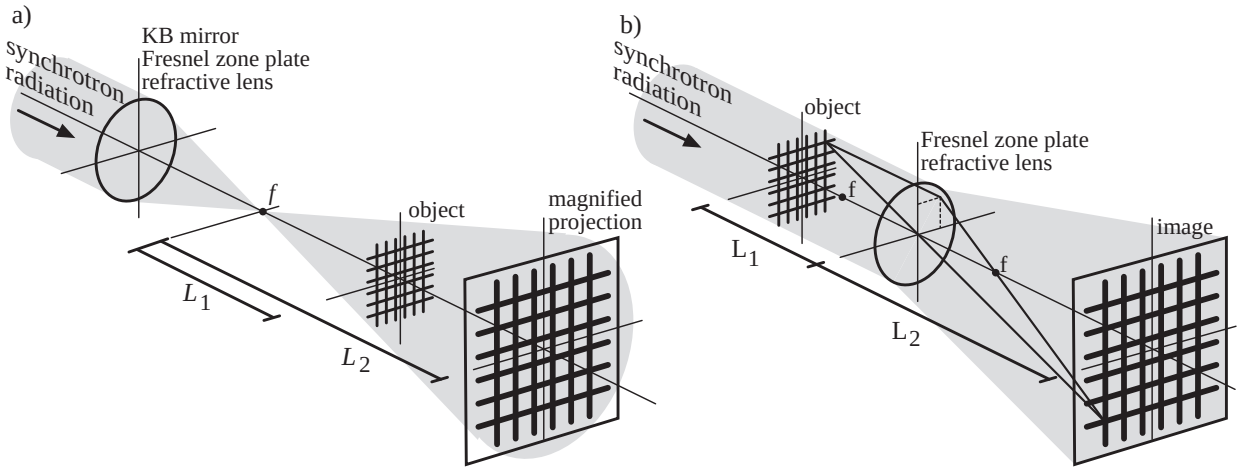

Figure 1. Schematic diagram of (a) hard x-ray magnifying projection and (b) full-field microscopy.

zone plate or refractive lens, can be used to image the object with magnification onto a position sensitive detector (Fig. 1(b)). Based on refractive x-ray lenses, we use this latter scheme to record magnified projection images that serve as input for high resolution tomographic imaging. We give an example of magnifying tomographic imaging with sub-micrometer resolution in section 3.

Full-field microscopy has the great advantage of recording large x-ray images of the object in parallel using two-dimensional position sensitive detectors, it is however, limited to contrast mechanisms based on x-ray transmission through the sample. In order to exploit other x-ray analytical techniques as contrast mechanisms, such as x-ray fluorescence, absorption spectroscopy, or x-ray scattering, the sample can be scanned though a small beam. These hard x-ray scanning microscopy techniques are comparatively slow, as they obtain the spatial distribution sequentially, they yield, however, information about the element distribution, chemical state, or local nano-structure of a sample. In section 4, an example is shown on how the local small-angle scattering cross-section can be reconstructed on a virtual slice through a specimen.

In both full-field and scanning microscopy and tomography, high resolution x-ray optics are needed to achieve high spatial resolution. In this article, parabolic refractive x-ray lenses are used for this purpose. An overview over these optics is given in the next section.

2. REFRACTIVE X-RAY OPTICS

Since their first experimental realization about a decade ago,[1] refractive x-ray lenses have developed quickly into a high end optic for x-ray microscopy applications. Over the years, there have been many different approaches to making refractive optics.[2–8]

Refraction of hard x-rays in matter is very weak and is described by the refractive index $n = 1 - \delta + i\beta$, where δ is the small positive index of refraction decrement ($\delta \approx 10^{-6}$ around 10 keV), and β describes attenuation. Since the refractive index for hard x-rays in matter is slightly smaller than unity, focusing optics have to have concave shape. Due to the extremely small δ, a refractive x-ray lens needs to have an effective curvature in the micrometer range to reach a focal distance in the meter range. Since it is difficult to fabricate a single lens with such a radius of curvature and large aperture, these optics are usually realized as a compound optic composed of a stack of a many individual lenses with moderate curvature (e. g., with radius of curvature of several hundred micrometers).[9]

As compared to visible light in glass, x-rays are attenuated significantly inside all materials as described by the imaginary part β of the refractive index. Thus, in order to achieve optimal transmission and a large aperture, it is crucial to reduce attenuation to a minimum by choosing lens materials with low atomic number

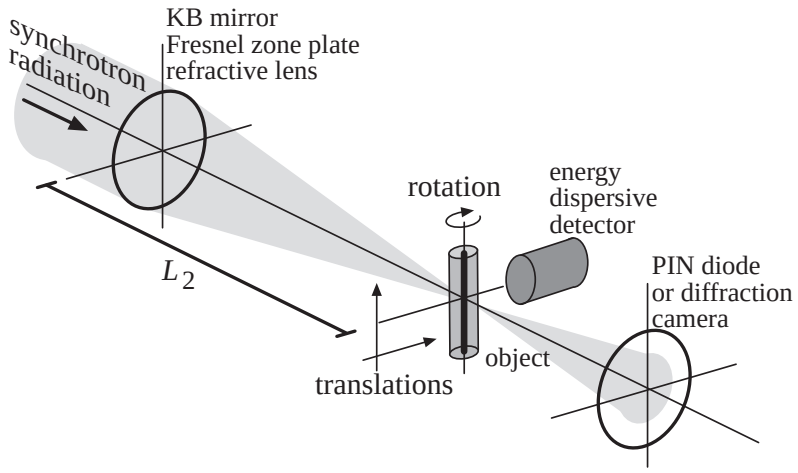

Figure 2. Schematic diagram of a setup for scanning microscopy.

Z, such as beryllium, boron, carbon, or compounds thereof. A detailed discussion of the lens properties and the requirements on lens materials are found elsewhere.[2,3,10]

As the radii of curvature of x-ray optics are usually comparable to or smaller than their aperture, the spherical approximation does not hold for these optics, and an aspherical lens shape is required to avoid strong aberrations. In a compound lens, each individual lens is thin (i. e., its focal length is significantly longer than its thickness). This implies that for optimal performance the lens surfaces should have parabolic shape. For undistorted imaging, rotationally parabolic lenses are ideal.[3,9,10] Rotationally parabolic refractive x-ray lenses made of aluminium and beryllium have been developed at Aachen University. Sofar, a spatial resolution of about 100 nm has been reached in full-field imaging with a beryllium objective lens.[11]

In order to generate very small foci at short distances from the synchrotron radiation source, nanofocusing refractive x-ray optics with a focal length in the centimeter range were developed.[12] Made by planar nanofabrication techniques, these optics focus in one dimension only, requiring one to cross two of them to generate a point focus. They are the basis for a hard x-ray scanning microscope that is currently being developed. This microscope will allow for tomographic scanning and can be operated in fluorescence, absorption, and scattering mode. Recently, a hard x-ray nanobeam with a lateral extension of 50 nm was generated with this setup.[13]

Refractive x-ray lenses are genuine imaging optics that can be used in analogy to glass lenses for visible light. They can be used for full-field imaging for example in x-ray microscopy (section 3) or for generating a small x-ray beam for example for scanning microscopy applications (section 4).

3. HARD X-RAY FULL-FIELD MICROSCOPY AND TOMOGRAPHY

Using the setup shown in Figure 1(b), a rotationally parabolic refractive x-ray lens can be used to image the sample onto a detector in a magnifying geometry. The sample is illuminated from the back by monochromatic hard x-rays from a synchrotron radiation source. The optic is placed behind the sample at a distance L_1 that is slightly larger than its focal distance f. The image is formed a distance $L_2 = L_1 f/(L_1 - f)$ behind the lens on a high resolution x-ray camera. The resulting magnification is $m = L_2/L_1 = f/(L_1 - f)$.

For incoherent illumination, the spatial resolution that can be achieved in this microscope is

$$d_t = 0.75\frac{\lambda L_1}{D_{\text{eff}}} = 0.75\frac{\lambda}{2NA}, \tag{1}$$

where λ is the x-ray wave length, D_{eff} is the effective aperture and $NA = D_{\text{eff}}/L_1$ is the numerical aperture of the objective lens in the microscope geometry.[3] For a refractive lens D_{eff} is slightly smaller than its geometric

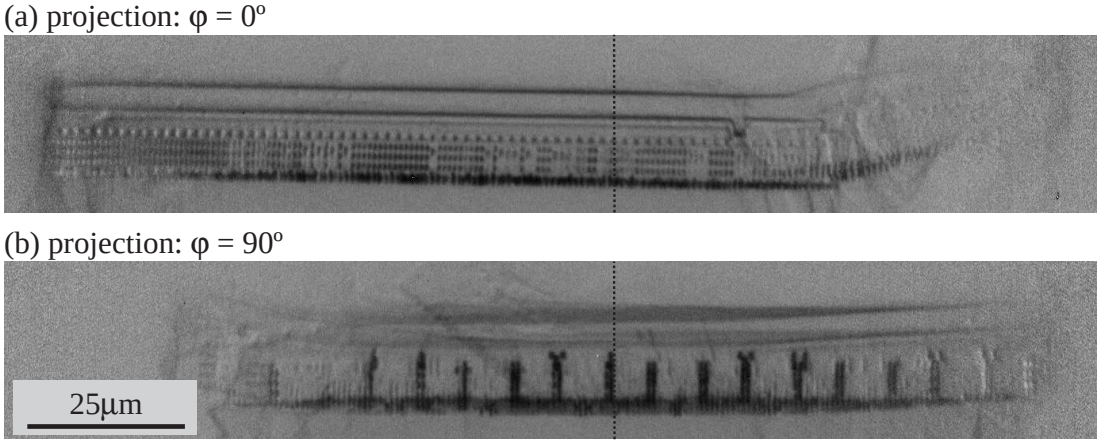

Figure 3. (a) and (b) show two x-ray micrographs of a fragment of an AMD K6 microprocessor used as a test structure. They are part of a tomographic scan and were recorded perpendicularly to each other. The rotation axis is depicted as a dashed line in both images.

aperture due to an increased attenuation of the x-rays in the outer (thicker) parts of the (concave) lens. Typically, the numerical aperture NA of beryllium parabolic refractive lenses lies in the range between 10^{-4} to 10^{-3}. In order to illuminate the sample incoherently and to match the numerical aperture of the optic, a diffuser (rotating random scatterer, e. g., boron carbide powder between two thin glass plates) is placed into the illuminating beam shortly before the sample.

While the small numerical aperture limits the spatial resolution d_t that can be achieved, it has the advantage of giving a large depth of field

$$d_l = 0.64\frac{\lambda}{NA^2} \approx \frac{d_t}{NA} \tag{2}$$

relative to the spatial resolution. This is favorable to tomographic imaging, since it allows one to image thick objects in sharp projection.

To acquire a tomogram, a large number of magnified images of the sample is recorded, rotating the sample around an axis perpendicular to the beam. Magnified tomography based on refractive x-ray lenses is illustrated using a piece of an AMD K6 microprocessor as a test object.[14] For the example given here, the x-ray full-field microscope was set up at beamline ID22 of the ESRF. Using a parabolic refractive x-ray objective lens made of aluminium with a focal length of $f = 1048$ mm at $E = 25$ keV, the sample was imaged with 20.9 fold magnification onto a high resolution x-ray camera ($L_1 = 1098$ mm, $L_2 = 23.02$ m). This microscope was used to record a tomogram of a $100 \times 150\mu\text{m}^2$ fragment of an AMD K6 microprocessor, which was prepared as a test object. 500 projections were recorded in an angular interval of 180° around the normal of the microprocessor's plane.

Figure 3(a,b) shows two projections through the microprocessor. The dashed vertical line indicates the rotation axis. The silicon wafer (at the bottom of each image) on which the processor is built gives almost no attenuation contrast (cf. schematic drawing of a microprocessor in Fig. 4(e)). The tungsten plug connects that make an electronic contact of the semiconductor devices with the first layer of aluminium interconnects is seen as the dark, structured horizontal line at the bottom. Within four layers of oxide, the tungsten plug vias are visible as dark vertical bars, making the electrical connection between aluminium interconnects that lie on different oxide layers. The silicon, the oxides and the aluminium interconnects all attenuate the x-rays very weakly and yield no absorption contrast above the noise level in this experiment. The contrast of these structures could be significantly increased by using phase contrast techniques.

The microprocessor was reconstructed tomographically using filtered backprojection. Prior to backprojection, unwanted motion of the rotation axis was compensated for numerically. Tomographic reconstruction is shown

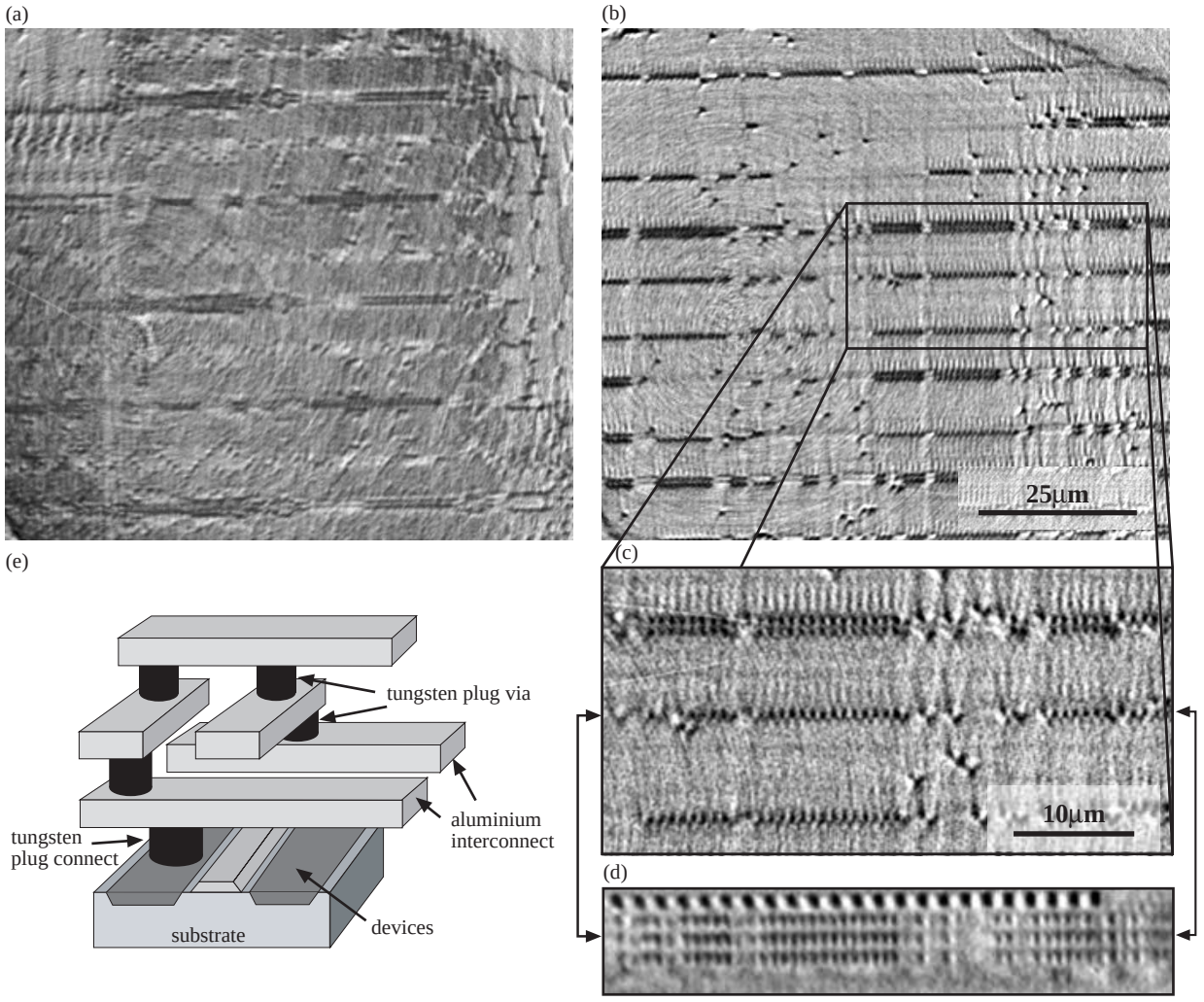

Figure 4. (a) Tomographic (horizontal) slice through the device layer of the microprocessor, (b) (horizontal) slice through the second layer of tungsten plug vias. (c) is a magnified view of the rectangular region in (b), (d) shows a vertical slice through the row of plug vias marked by the arrows in (c). (e) Schematic sketch of the structure of a microprocessor. The devices are structured lithographically onto the substrate and connected by tungsten plug connects to the first layer of aluminium interconnects. Several layers of aluminium interconnects are connected by tungsten plug vias.

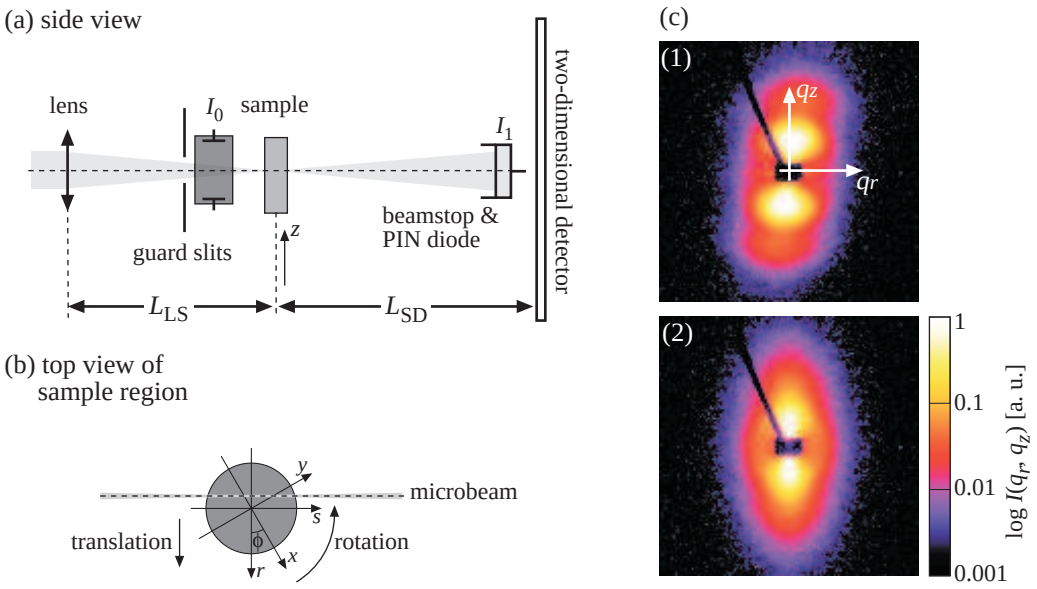

Figure 5. (a) Side view of the setup for micro-small-angle scattering tomography. (b) Top view of the sample region. (c) Small-angle x-ray scattering patterns of an injection-molded polyethylene rod (cylinder axis parallel to the rotation axis z), recorded with an x-ray microbeam impinging (1) periferally and (2) centrally.

in Figure 4. The spatial resolution in the reconstruction is about 0.4μm.

In order to obtain high resolution tomograms, the projection images must be free of distortion and the setup must have sufficient mechanical stability. Most important is the mechanical stability of the sample stage that must allow for a rotation of the sample with small eccentricity and wobble.

While magnified tomographic imaging with hard x-rays has been shown to yield sub-micrometer resolution in a few demonstration experiments, it is still under development and not routinely available to users of synchrotron radiation sources. In a more recent experiment using a beryllium objective lens at the Advanced Photon Source (7-ID), the smallest features of a modern Athlon XP 2000 microprocessor could be resolved in projections. However, tomographic reconstruction of this sample is difficult, as refraction effects inside the sample are significant, requiring a more sophisticated tomographic model.

4. TOMOGRAPHIC IMAGING OF THE LOCAL NANOSTRUCTURE BY SMALL-ANGLE X-RAY SCATTERING TOMOGRAPHY

X-ray scattering is the most prominent method for structure determination of (crystalline) materials down to the atomic level. The scattering signal around the forward direction, the so-called small-angle x-ray scattering (SAXS) regime, reveals the structure of a specimen on scales of nanometers to several hundred nanometers. In this regime a lot of structural information can be obtained, also from non-crystalline and disordered samples. By combining small-angle scattering with scanning microscopy, the variation in the local nanostructure of a heterogeneous specimen can be investigated. By combining small-angle scattering with scanning tomography, local nanoscale information at each location on a virtual section through a specimen can be obtained.[15]

The setup for small-angle scattering tomography is shown in Figure 5(a,b). Using an x-ray optic, a microbeam is generated at the sample position. The sample is scanned through this monochromatic microbeam in translation and rotation. To record a single tomographic projection, the sample is scanned through the microbeam in translation. At each position of this scan, the transmitted radiation I_1 is recorded by a PIN-diode that serves as beamstop for a diffraction camera that records the two-dimensional small-angle scattering pattern $I_{(q_r,q_z)}(r,\phi)$ from the sample. After the completion of a translational scan, the sample is rotated by an integer fraction of

180° and the next projection is recorded. This procedure is repeated until the sample has completed a 180° rotation. In general the small-angle scattering pattern $I_{(q_r,q_z)}(r,\phi)$ depends on the sample position r, orientation ϕ, and the momentum transfer (q_r, q_z). The guard slit (Fig. 5(a)) removes scattered radiation from all optical components upstream, and the incident beam is monitored by an ionization chamber I_0 behind the guard slit.

As an example, a SAXS tomogram is shown of a polyethylene rod that was made by injection molding and that was subsequently stretched at elevated temperatures. Details of this experiment can be found elsewhere.[15,16] The rod was scanned with a microbeam generated with beryllium parabolic refractive x-ray lenses at the DORIS III beamline BW4 at DESY in Hamburg. 101 projections with 69 translational steps each were recorded, acquiring at each position (r,ϕ) of the scan the incident flux I_0, the transmitted flux I_1, and the SAXS pattern $I_{(q_r,q_z)}$. Fig. 5(c) shows two SAXS patterns of the polyethylene rod, recorded with the x-ray beam impinging (1) periferally and (2) centrally.

The transmission signal I_1 measured by the PIN-diode can be readily used to determine the attenuation coefficient $\mu(x,y)$. It can be easily reconstructed from the transmission tomographic data

$$I_1 = I_0 \exp\left\{-\int ds'\ \mu[x(s',r), y(s',r)]\right\} \tag{3}$$

by filtered backprojection. Fig. 6(left) shows the reconstructed attenuation coefficient of the polyethylene rod. It appears homogeneous, with a homogeneous mass density of $\rho = 0.88 \pm 0.04$ g/cm^3. From attenuation contrast alone it would be concluded that the sample is homogeneous.

The reconstruction of the SAXS data is more involved. Assuming the first Born approximation, the SAXS pattern at a given position (r,ϕ) within the tomographic scan is given by

$$I_{(q_r,q_z)}(r,\phi) = I_0 \int ds\ f(\phi,s,r) p_{q_r,q_z,\phi}(x,y) g(\phi,s,r), \tag{4}$$

where $f(\phi,s,r) = \exp\{-\int_{-\infty}^{s} ds'\ \mu[x(s',r), y(s',r)]\}$ is the attenuation of the incident beam as it propagates through the sample to a point of scattering (s,r). At the point (s,r) the scattering of the beam is described by $p_{q_r,q_z,\phi}(x,y)$, which in general depends on the angle ϕ for $q_r \neq 0$. $g(\phi,s,r) = \exp\{-\int_{-\infty}^{s} ds'\ \mu[x(s',r), y(s',r)]\}$ describes the attenuation of the scattered beam in the forward direction. Here it was assumed, that the scattering angles are small. f and g can be combined and pulled out of the integral in eq. (4). Using eq. (3), equation (4) can be simplified:

$$I_{(q_r,q_z)}(r,\phi) = I_1 \int ds\ p_{q_r,q_z,\phi}(x,y). \tag{5}$$

This equation shows that in order to correct for attenuation inside the sample, the scattering signal $I_{(q_r,q_z)}$ needs to be normalized by the transmitted signal I_1. Since $p_{q_r,q_z,\phi}$ in general depends on the rotation angle ϕ, the acquired tomographic projections in general do not provide sufficient information to solve the tomographic problem for all (q_r,q_z). For $q_r = 0$, i. e., for $\vec{q}$ along the rotation axis, however, the diffraction pattern $p_{0,q_z,\phi}$ is independent of ϕ. Therefore, standard tomographic methods can be used to reconstruct the scattering cross section for this restricted set of data. The integral of the cross section along this line ($q_r = 0$) is shown in the right reconstruction in Fig. 6. As opposed to the attenuation coefficient, the reconstructed SAXS cross sections vary strongly over the virtual section through the sample, clearly showing a core-shell structure of the rod.

If, in addition, the SAXS cross section is rotationally symmetric with respect to the rotation axis, then the full cross section p_{q_r,q_z} is independent of ϕ and can be reconstructed for any (q_r,q_z). In the given example, the scattering from the polyethylene rod has approximately this symmetry, showing a strong fibre texture along the rotation axis (Fig. 5(c)). This allows one to reconstruct the full SAXS cross sections at each point on the virtual slice through the sample. Fig. 6 shows the SAXS cross sections reconstructed at five different locations inside the sample labeled (a) through (e). The clear diffraction peaks at the periphery of the rod (Fig. 6(a,b)) indicate an almost latticelike arrangement of alternating crystalline and amorphous polyethylene lamellae. The bright shell in Fig. 6(right) is dominated by more or less diffuse scattering of uncorrelated domains of stacked crystalline and amorphous lamellae of varying thickness (Fig. 6(c,d)). In the center, discrete scattering is observed again (Fig. 6(e)). A detailed analysis of the reconstructed diffraction patterns can be made using the multidimensional chord distribution function method (CDF).[16]

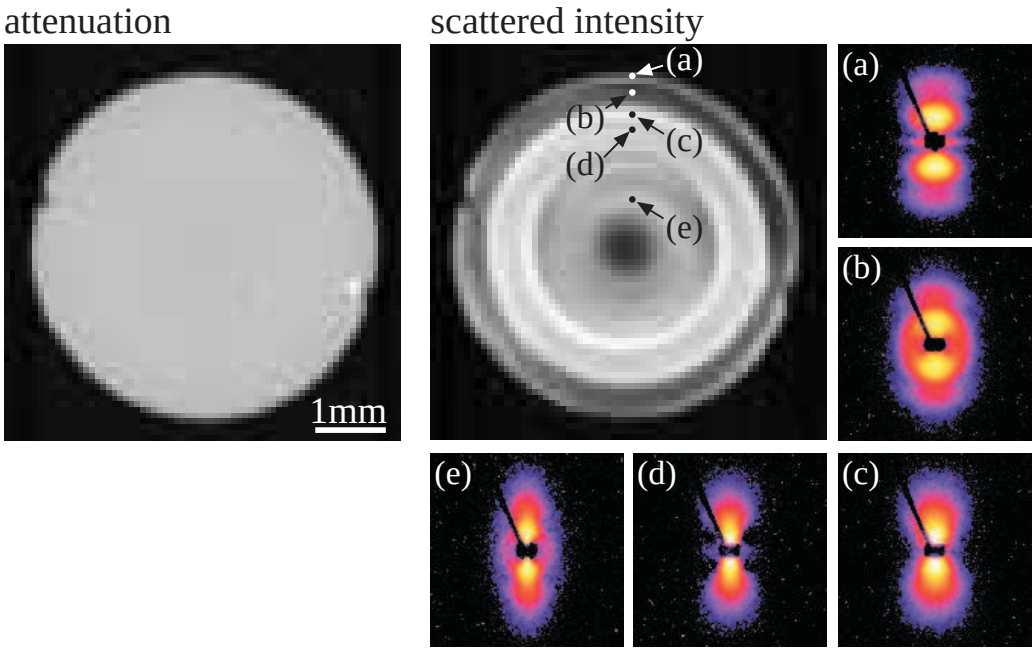

Figure 6. (Left) reconstructed attenuation coefficient μ and (right) integral small-angle scattering cross section $p_{(0,q_z)}(x,y)$ along the q_z-direction parallel to the tomographic rotation axis. For several locations marked (a) through (e) the reconstructed SAXS cross sections are shown.

5. CONCLUSION

Parabolic refractive x-ray lenses are high quality imaging optics that can be used for full-field and scanning microscopy. A full-field microscope based on rotationally parabolic refractive x-ray lenses was used to record a tomogram of a fragment of a microprocessor. The tomographic reconstruction yields its three-dimensional structure with a spatial resolution of 410 nm. In addition, refractive x-ray lenses can be used to generate an intensive hard x-ray microbeam that can be used for scanning microscopy and tomography. As an example, we have used small-angle x-ray scattering tomography to obtain the local nanostructure on a virtual section through a polyethylene rod. The spatial resolution in this example was about 80 μm, adapted to the sample diameter of about 6 mm. Refractive x-ray lenses can be used to generate nanobeams with a lateral extension down to about 50 nm.[13] Based on these optics, a prototypical hard x-ray nanoprobe station is being developed that will allow one to perform similar scanning microscopy and tomography experiments with sub-100 nm resolution.

ACKNOWLEDGMENTS

The magnified tomogram was recorded during the long term project MI-506 at ESRF. The construction of the full-field microscope was funded by the German Ministry of Education and Research (BMBF) under grant number 05KS1PAB/5. We thank R. Döhrmann and M. Dommach for their excellent support during the SAXS-tomography experiments carried out at beamline BW4 at DESY in Hamburg. The development of refractive x-ray lenses and of a hard x-ray nanoprobe based thereon is supported by the German Ministry of Education and Research (BMBF) under grant number 05KS4PA1/9.

REFERENCES

1. A. Snigirev, V. Kohn, I. Snigireva, and B. Lengeler, "A compound refractive lens for focusing high energy x-rays," *Nature (London)* **384**, p. 49, 1996.
2. B. Lengeler, J. Tümmler, A. Snigirev, I. Snigireva, and C. Raven, "Transmission and gain of singly and doubly focusing refractive x-ray lenses," *J. Appl. Phys.* **84**(11), pp. 5855–5861, 1998.

3. B. Lengeler, C. Schroer, J. Tümmler, B. Benner, M. Richwin, A. Snigirev, I. Snigireva, and M. Drakopoulos, "Imaging by parabolic refractive lenses in the hard x-ray range," *J. Synchrotron Rad.* **6**, pp. 1153–1167, 1999.
4. Y. Kohmura, M. Awaji, Y. Suzuki, T. Ishikawa, Y. I. Dudchik, N. N. Kolchewsky, and F. F. Komarow, "X-ray focusing test and x-ray imaging test by a microcapillary x-ray lens at an undulator beamline," *Rev. Sci. Instrum.* **70**(11), pp. 4161–4167, 1999.
5. J. T. Cremer, M. A. Piestrup, H. R. Beguiristain, C. K. Gary, R. H. . Pantell, and R. Tatchyn, "Cylindrical compound refractive x-ray lenses using plastic substrates," *Rev. Sci. Instrum.* **70**(9), 1999.
6. B. Cederström, R. N. Cahn, M. Danielsson, M. Lundqvist, and D. R. Nygren, "Focusing hard X-rays with old LP's," *Nature* **404**, p. 951, 2000.
7. V. Aristov, M. Grigoriev, S. Kuznetsov, L. Shabelnikov, V. Yunkin, T. Weitkamp, C. Rau, I. Snigireva, A. Snigirev, M. Hoffmann, and E. Voges, "X-ray refractive planar lens with minimized absorption," *Appl. Phys. Lett.* **77**(24), pp. 4058–4060, 2000.
8. B. Nöhammer, J. Hoszowska, A. K. Freund, and C. David, "Diamond planar refractive lenses for third- and forth-generation X-ray sources," *J. Synchrotron Rad.* **10**, pp. 168–171, 2003.
9. B. Lengeler, C. G. Schroer, M. Kuhlmann, B. Benner, T. F. Günzler, O. Kurapova, F. Zontone, A. Snigirev, and I. Snigireva, "Refractive x-ray lenses," *J. Phys. D: Appl. Phys.* **38**, pp. A218–A222, 2005.
10. B. Lengeler, C. G. Schroer, M. Richwin, J. Tümmler, M. Drakopoulos, A. Snigirev, and I. Snigireva, "A microscope for hard x-rays based on parabolic compound refractive lenses," *Appl. Phys. Lett.* **74**(26), pp. 3924–3926, 1999.
11. C. G. Schroer, M. Kuhlmann, B. Lengeler, T. F. Günzler, O. Kurapova, B. Benner, C. Rau, A. S. Simionovici, A. Snigirev, and I. Snigireva, "Beryllium parabolic refractive x-ray lenses," in *Design and Microfabrication of Novel X-Ray Optics*, D. C. Mancini, ed., *Proceedings of the SPIE* **4783**, pp. 10–18, SPIE, (Bellingham), 2002.
12. C. G. Schroer, M. Kuhlmann, U. T. Hunger, T. F. Günzler, O. Kurapova, S. Feste, F. Frehse, B. Lengeler, M. Drakopoulos, A. Somogyi, A. S. Simionovici, A. Snigirev, I. Snigireva, C. Schug, and W. H. Schröder, "Nanofocusing parabolic refractive x-ray lenses," *Appl. Phys. Lett.* **82**(9), pp. 1485–1487, 2003.
13. C. G. Schroer, O. Kurapova, J. Patommel, P. Boye, J. Feldkamp, B. Lengeler, M. Burghammer, C. Riekel, L. Vincze, A. van der Hart, and M. Küchler, "Hard x-ray nanoprobe based on refractive x-ray lenses," *Appl. Phys. Lett.* **87**(12), p. 124103, 2005.
14. C. G. Schroer, J. Meyer, M. Kuhlmann, B. Benner, T. F. Günzler, B. Lengeler, C. Rau, T. Weitkamp, A. Snigirev, and I. Snigireva, "Nanotomography based on hard x-ray microscopy with refractive lenses," *Appl. Phys. Lett.* **81**(8), pp. 1527–1529, 2002.
15. C. G. Schroer, M. Kuhlmann, S. V. Roth, R. Gehrke, N. Stribeck, A. Almendarez-Camarillo, and B. Lengeler, "Mapping the local nanostructure inside a specimen by tomographic small angle x-ray scattering," *Appl. Phys. Lett.* **88**(16), p. 164102, 2006.
16. N. Stribeck, A. Almendarez-Camarillo, U. Nöchel, C. Schroer, M. Kuhlmann, S. V. Roth, R. Gehrke, and R. K. Bayer, "Volume-resolved nanostructure survey of a polymer part by means of saxs microtomography," *Macromol. Chem. Phys.* **207**, pp. 1139–1149, 2006.